https://doi.org/10.1016/j.surfcoat.2020.125491

# Influence of ion irradiation on the nanomechanical properties of thin alumina coatings deposited on 316L SS by PLD

A. Zaborowska[a,*)], Ł. Kurpaska[a)], E. Wyszkowska[a)], M. Clozel[a)], M. Vanazzi[b,c)], F. Di Fonzo[b)], M. Turek[d)], I. Jóźwik[a,e)], A. Kosińska[a)], J. Jagielski[a,e)]

[a)] *National Center for Nuclear Research, NOMATEN CoE MAB+ Division, A. Soltana 7, 05-400 Otwock-Swierk, Poland*

[b)] *Center for Nano Science and Technology @PoliMi, Istituto Italiano di Tecnologia, Via Giovanni Pascoli 70/3, 20133 Milano, Italy*

[c)] *Dipartimento di Energia, Politecnico di Milano, Via Ponzio 34/3, 20133, Milano, Italy*

[d)] *Institute of Physics, Maria Curie Skłodowska University, pl. M. Curie-Skłodowskiej 1, 20-031 Lublin, Poland*

[e)] *Institute of Electronic Materials Technology, st. Wólczynska 133, 01-919 Warsaw, Poland*

**corresponding author: agata.zaborowska@ncbj.gov.pl, Phone: (+48) 22 273 1061, Fax: (+48) 22 273 1061*

**Abstract**

In terms of nuclear applications, ceramics are seen as a particularly promising class of materials due to their chemical inertness and relatively high radiation resistance. However, since ceramics exhibit high brittleness at low homologous temperatures, the application of monolithic ceramics as structural components of nuclear power plants is rather limited. On the other hand, deposition of ceramic coatings on a metallic substrate may result in an excellent combination of mechanical, corrosion and radiation properties (especially at high temperature). In this work, $Al_2O_3$ coatings deposited by Pulsed Laser Deposition (PLD) on 316L SS substrate at room temperature were investigated. In order to simulate the influence of neutrons, alumina-coated and 316L SS samples were irradiated at room temperature with 250 keV $Au^+$ and 150 keV $Fe^{2+}$ ions, respectively. The influence of ion irradiation on nanomechanical properties of the studied materials was investigated by means of Nanoindentation (NI) technique. Based on the obtained results, nanomechanical properties as a function of radiation damage level were determined and linked to the results of Grazing Incidence X-Ray Diffraction (GIXRD) analysis and other structural data available in the literature. Irradiation-induced softening and hardening were observed, respectively, in the

alumina coating and 316L SS. Reported differences, which are induced by the irradiation effects, are considered to be due to the different microstructures of the pristine materials.

**Keywords:** Nanoindentation, Ion irradiation, Nanoceramic coating, Alumina, Stainless steel,

**Abbreviations:**

PLD - Pulsed Laser Deposition

HLM - Heavy Liquid Metal

## 1. Introduction

Generation IV nuclear reactors have many advantages over currently operated reactors and are foreseen to help to meet the world's future energy needs. Aforesaid advantages include improvements in four broad areas: (i) sustainability, (ii) economics, (iii) safety and reliability and (iv) proliferation resistance and physical protection [1]. Among Generation IV fast reactor systems, Lead-Cooled Fast Reactor (LFR) is considered to be one of the most promising technologies [1]. One of the issues associated with its deployment (and the deployment of other technologies, too) is the lack of sufficiently reliable materials capable of withstanding extremely harsh operating conditions, particularly for core components. These conditions, determined by design, include high temperatures, intense neutron radiation field and contact with highly corrosive non-aqueous coolant. For example, several groups [1–3] pointed out that fuel cladding under nominal operating conditions in ALFRED (Advanced Lead-cooled Fast Reactor European Demonstrator) and ELFR (European Lead-cooled Fast Reactor) will be exposed to temperatures reaching 550 ºC, whereas neutron fields will cause clad damage up to 100-200 dpa.

The majority of materials selected for components of ALFRED and ELFR are austenitic steels (AISI316L and 15-15Ti) [1,2]. Specifically, 15-15Ti SS and T91 (ferritic/martensitic steel) were selected for the fuel cladding in ALFRED and ELFR, respectively [2]. However, it is well known that the dominant steel elements (like Fe, Cr or Ni) in liquid lead are highly susceptible to the dissolution effect [1,2]. Therefore, direct contact between liquid lead and steel components must be prevented during the whole operation cycle of the component. The common corrosion mitigation strategy for the considered steels consists in the controlled addition of oxygen to the liquid metal, to cause the in-situ formation of an oxide scale during operation [2]. However, it has been shown that for 316L SS at temperatures above approx. 480 ºC, this protection method becomes ineffective [2]. Likewise 15-15Ti steel, despite oxide

formation, is expected to suffer from dissolution during long-term operation at 550 ºC in Pb [2]. At the same time, the T91 f/m steel is resistant to dissolution attack in foreseen operating conditions, but in turn oxidation (resulting in a reduction of heat conductivity) becomes a major problem [2]. Hence, for fuel cladding in LFR an alternative approach to protect against HLM corrosion is required.

A very promising solution is the use of ceramic coatings, most of which are practically insoluble in liquid lead and lead alloys. Among others, the Istituto Italiano di Tecnologia (IIT) has developed thin alumina coatings deposited by PLD technique. In [4], authors have shown that $Al_2O_3$-coated 15-15Ti steel samples exposed to LFR relevant corrosion conditions (i.e. 550 ºC, $10^{-8}$ wt. % oxygen) during 1000h and 4000h (for ion-irradiated and pristine samples, respectively) do not interact with liquid lead. In addition to that, further research of this group has shown that the PLD-grown alumina coating is characterized by a number of other excellent features, namely: (i) uniform, fully dense and compact structure [4–8]; (ii) electrical insulating properties [6]; (iii) unusual combination of metal-like mechanical properties (Young's modulus E = 195 ± 9 GPa, υ = 0.29 ± 0.02) and ceramic hardness (H = 10 ± 1 GPa) [5]; (iv) great wear resistance (0.051 value of H/E ratio is comparable with the ratios of superhard nanocomposite coatings dedicated to tribological applications) [5]; (v) strong interfacial bonding between coating and substrate [4,5]; (vi) resistance to thermal cycling [4]; (vii) high hydrogen and deuterium permeation reduction factors (PRFs) which are close to $10^5$ at 650 ºC (even after electron irradiation) [6,7]; (viii) excellent behavior under ion radiation (up to 450 dpa) [4,9,10].

The determination of the radiation resistance of materials dedicated to nuclear applications is one of the crucial issues. Only few works in the literature have investigated the radiation endurance in PLD-grown $Al_2O_3$. Previously published data [9,10] suggest that irradiation induces full crystallization of the as-deposited structure (consisting of amorphous matrix and $\gamma$-$Al_2O_3$ nanocrystalline domains) which is followed by grain growth. Crystallization results

in a prominent hardness increase. Subsequent grain growth induces softening of the material, thereby partially reducing the initial hardness increase. To summarize, the phenomena here reported result in a general hardening, due to appearance of crystalline phases (in comparison to the virgin specimen).

Traditionally, radiation effects studies consist in material irradiation in nuclear test reactors and subsequent characterization of irradiated samples. However, this procedure is associated with extraordinarily high costs and long exposure times (radiation damage rate in test reactors does not exceed 20 dpa/year) [11]. Furthermore, as expected, samples become activated after being kept in the core, and hence access to special facilities (i.e. hot cells) and compliance with strict radioactive material handling regulations are required. This involves additional costs. Consequently, methods of simulating neutron irradiation damage in materials have been developed in recent decades. Among them, the best-developed, widely and successfully applied technique is ion irradiation. Utilization of ions brings a number of benefits compared to neutron radiation, namely: cost reduction, shorter time needed to modify the materials (damage rates can reach up to $10^4$ times that of the reactor), no or negligible activation of samples, and better control of irradiation conditions [11–14].

Due to the limited available data concerning radiation response of the discussed coating and of amorphous ceramics in general, further systematic studies on the behavior of PLD-grown $Al_2O_3$ under irradiation are highly desired. Furthermore, in the planned operating environment, neutrons will penetrate material significantly below the thin coating. Thus, the evaluation of irradiation resistance of the substrate and the interface between coating and substrate is equally indispensable. There are numerous published reports on the microstructural evolution of 300 series stainless steels subjected to ion irradiation. On the other hand, according to our knowledge, only few works [15–17] were focused on the assessment of the evolution of mechanical properties of stainless steels exposed to ion

irradiation. Such deficiencies relate in particular to comprehensive investigations, over a wide range of doses, including high levels of damage.

In spite of the many advantages, using ion irradiation as a surrogate for neutron radiations does have some serious drawbacks. One of these is the very limited volume of the affected material. The thickness of the layer penetrated by ions (which depends on the material and the nature and energy of selected ions) usually does not exceed a hundreds of nanometers [18]. For this reason, conventional methods of determination of mechanical properties in the case of ion irradiated materials are clearly inapplicable. Therefore, the use of other (predominantly challenging) methods to reliably extract mechanical properties from such small volumes is required. One of such methods designed for the investigation of small or/and thin samples, layers and coatings is nanoindentation. Over the past three decades nanoindentation became a viable and widely used non-destructive technique [19,20]. There have been a number of studies [16,17,21–24] successfully using the combination of described techniques (ion irradiation and nanoindentation) as a means to evaluate the influence of neutron irradiation on mechanical properties of various materials.

For this reason, in this study, the influence of ion irradiation on nanomechanical properties of thin alumina coatings deposited by PLD at RT on 316L SS and bulk 316L SS was investigated. Afterwards, obtained nanomechanical characteristics of the materials were critically compared with the available structural data. It is believed that the obtained results will contribute to the current knowledge related to the materials foreseen as structural components in future advanced nuclear reactors.

## 2. Materials and methods

### 2.1. Materials preparation

Steel samples (10x10 mm) were cut by means of WEDM (Wire Electrical Discharge Machining) from an annealed sheet with a thickness of 0.9 mm provided by Goodfellow.

After cutting, samples were polished by using SiC abrasive grinding papers (grit size up to 1200), liquid diamond suspensions (with grain sizes 9 μm, 6 μm and 3 μm) and a finally colloidal silica suspension (0,06 μm grain size). As the success of nanoindentation investigations of thin layers depends to a large extend from the quality of the surface, particular attention was paid to obtain flat and smooth sample. Half of the samples prepared in this way were used as substrates for alumina coatings. Thin coatings were grown by PLD technique at room temperature. Details of the deposition process can be found elsewhere [5]. Surface roughness of materials was evaluated using Hommelwarke LV-50 device. One SS sample and one alumina-coated sample were selected. Five measurements on 0,5 mm distance on each sample were performed. The average roughness values $R_a$ of the alumina and steel samples were 15 and 10 nm, respectively. Since ion irradiation can modify the surface roughness, measurements were repeated after the implantation process. The average roughness values $R_a$ of the alumina-coated and steel samples after ion-irradiation up to 50 dpa were 20 and 10 nm, respectively. It is worth mentioning that the resolution of the device is ~10 nm, so either the sputtering effect does not play a role at this energy, or is well below the instrumental resolution.

## 2.2. Ion irradiation

### 2.2.1. 316L SS

The as-prepared bulk samples of 316L SS were irradiated at room temperature with 150 keV $Fe^{2+}$ ions. The use of self-ion irradiation allowed to eliminate the effect of impurity. Ion beam current density was limited to 100 nA/cm$^2$ to minimize heating of the samples. During irradiation, the pressure in irradiation chamber was kept ~$10^{-6}$ mbar.

### 2.2.2. $Al_2O_3$ coating on 316L SS

The as-deposited $Al_2O_3$ coated samples on 316L SS were irradiated at room temperature with 250 keV $Au^+$ ions. The type and energy of ions were selected so that the microstructural

evolution under ion irradiation is comparable to structure modifications induced by neutron irradiation. Other studies [10,25] have shown that in order to simulate neutron damage in oxide ceramics, ions characterized by low ENSP (electronic-to-nuclear stopping) ratio should be used. The calculated ENSP ratio in fast fission reactor is around 4 [10,25]. In addition, a low absolute electronic energy loss component (preferably below 9.5 ± 1.5 keV/nm) is desirable [10,26–28]. This is related to the high sensitivity of ceramic insulators to ionizing radiation. For the given irradiation conditions, the maximum ionizing component of the irradiation spectrum is below 2,5 keV/nm, while the ENSP ratio through the irradiation depth is below 1,5. Implantations were performed using an ion implanter equipped with an arc discharge plasma ion source with internal evaporator. In order to avoid significant heating of the samples during the irradiation, ion current density was kept below 100 nA/cm$^2$. The pressure inside the target chamber was ~$10^{-6}$ mbar during the irradiation.

### 2.2.3. SRIM calculations

For both alumina-coated and steel samples, irradiation fluences were chosen so that they correspond to damage levels of about 0,5; 1; 3; 5; 10; 25 and 50 dpa. The nominal displacement damages were taken at their peak damages. The damage profiles (Fig. 1.) were obtained by using SRIM (The Stopping and Range of Ions in Matter) software. The radiation damage ranges were calculated to be 180 and 60 nm for steel and alumina-coated samples, respectively.

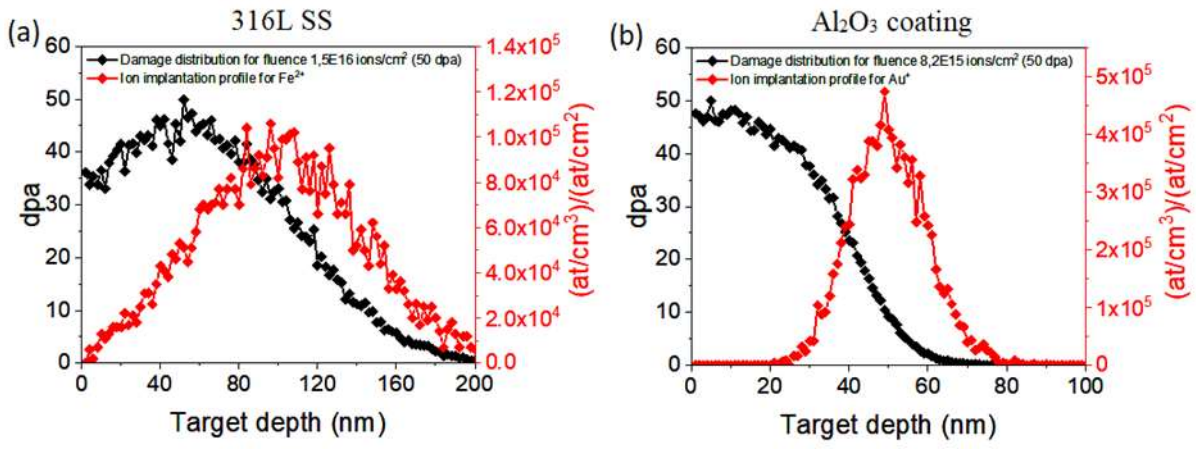

Fig. 1. Simulated irradiation damage (in dpa) as a function of target depth for: (a) 150 keV $Fe^{2+}$ ions in 316L SS; (b) 250 keV $Au^{+}$ ions in $Al_2O_3$ coating (1 μm thickness).

### 2.3. SEM

Scanning Electron Microscopy (SEM) observations were performed using Hitachi SU8230, Zeiss Auriga 60 and Zeiss EVO systems. The alumina-coated samples were examined for surface morphology and thickness of the layer, while the steel samples were etched and microstructure was observed. The alumina-coated samples chosen for surface observations prior the testing were covered with a thin layer of conductive material (chromium).

### 2.4. Grazing Incidence X-Ray diffraction (GIXRD)

GIXRD method was used to study the phase stability of PLD-grown alumina coating under ion-irradiation. X-ray diffraction measurements were carried out with Cu-Kα radiation (λ≈1,5418 Å) by Rigaku SmartLab X-ray diffractometer. The X-ray tube was operated at 40 kV and 30 mA. The diffraction patterns were collected in parallel beam (PB) mode with an incidence angle α of 0,5 ° and in the range from 20 ° to 80 ° of 2θ angle. Phase analysis was carried out using the Rigaku PDXL program and the ICDD database PDF4 + 2018. The mean penetration depth τ was calculated based on the equation [29]:

$$\tau_x = \frac{-ln(1-G_x)}{\mu\left(\frac{1}{sin\alpha}+\frac{1}{\sin(2\theta-\alpha)}\right)^{-1}}$$

where $\tau_x$ and $G_x$ correspond to the fraction of the radiation absorbed. Here $G_x$ is defined as $G_x$=1-1/10=0,9.

For the selected measurement parameters, the mean penetration depth in alumina was estimated to be about 2μm. Therefore, given the thickness of the investigated coating and the depth of the ion-modified layer, a signal contribution from steel substrate and unmodified

coating volume is expected. Nevertheless, in the event of phase transition, the differences between virgin and irradiated samples would be visible.

### 2.5. Nanoindentation

The goal of the nanomechanical tests was to evaluate the influence of ion irradiation on mechanical properties of studied materials. Both materials in eight states (virgin and ion irradiated to damage levels of 0,5; 1; 3; 5; 10; 25 and 50 dpa) were tested. Studies were performed by using NanoTest Vantage System provided by Micro Materials Ltd (MML). Measurements were done at room temperature with a diamond Berkovich indenter using load-controlled mode in line type experiment, with 10 forces (in the range from 0,2 to 4 mN and 20 mN for 316L SS and alumina-coated samples, respectively). Each indentation was repeated 15 times, with an interval of 50 μm. Before performing the main measurements, in order to minimize errors related to imperfect shape of the indenter, for each depth, the diamond area function (DAF) was determined using fuzed-silica as a reference. Hardness (H) and reduced Young's modulus ($E_r$) were calculated from the unloading data, according to the Oliver and Pharr model [30]. To convert reduced Young's modulus to Young's modulus, Poisson ratios of 0,27 [31] and 0,29 [5] were taken for 316L SS and $Al_2O_3$ coating, respectively. For presentation purposes, all recorded load-displacement curves set out in this paper were fitted by using MML software.

In order to conduct nanoindentation research in a reliable manner, it is essential to follow the best-practice guidelines. The general rule adopted from the literature states that the indenter penetration depth in nanoindentation test shall be within 10-20% of the thickness of the measured layer [18,23]. However, this value depends from the yield strength of the material [32] and can be equal even to 40-50% of the penetration depth [12,33,34]. This should ensure that the recorded response comes only from the measured layer. However, in case of nanoindentation studies of irradiated layers this limitation often leads to penetration

depths of several nanometers and thus to high measurements errors. For this reason, in certain cases the above limit is exceeded. In such cases, the aim is to ensure that nanoindentation meets two criteria: (i) the indents are as deep as possible to minimize the indentation size effect (ISE), the impact of surface roughness, as well as the impact of indenter tip shape imperfection; and (ii) the indents are as shallow as possible to reduce the signal from the unmodified volume of the material [18]. This approach requires preliminary nanoindentation tests over a wide range of indentation depths. Based on the performed studies, the optimal indentation depth and force were selected. It should be noted that in case of exceeding of described percent limit, plastic zone associated to the indentation is not contained entirely within the tested layer. Therefore, some contribution from the substrate may appear. For this reason, obtained mechanical results are somewhat affected and a very careful data interpretation is required. It is advisable that measurements carried out in this way are used for comparative research rather than for determining the actual properties of the tested materials. There are also some alternative methods which rely on mathematical modeling of the film–substrate systems and enable extraction of the film-only hardness value [35].

## 3. Results and discussion

### 3.1. SEM

The microstructure of 316L SS consisting of fine austenitic grains is shown in Fig. 2a. Fig. 2b. presents the cross-section of the investigated $Al_2O_3$ coating. Fig. 2c. and Fig. 2d. show the surface morphology of virgin and ion-irradiated coating. The thickness of the as-deposited coating was estimated based on the cross-sectional view as equal to ~1μm. No cracks or delamination on the interface between coating and substrate were observed. The coating is uniform and fully dense, its surface is smooth (as mentioned in Section 2.1., the average roughness value $R_a$ of the as-deposited alumina is 15 nm) and free of discontinuities.

Observations are consistent with [4–6] and confirm that PLD process is fairly mature and characterized by high reproducible results. No significant differences are observed between virgin and ion-modified surface.

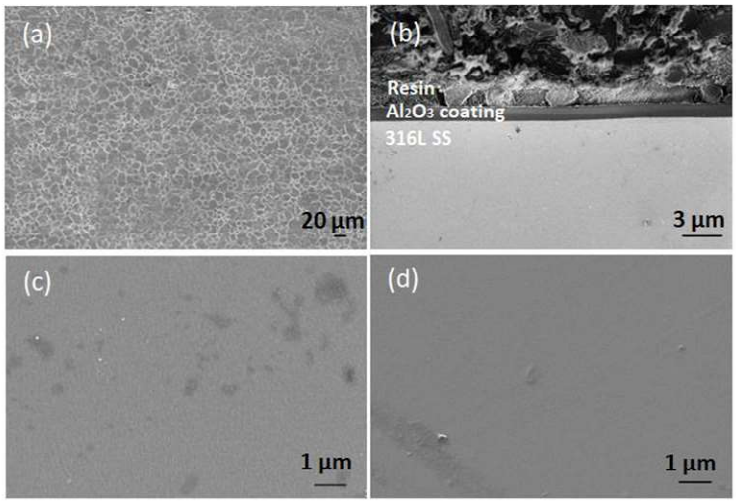


Fig. 2. SEM images of: (a) etched 316L SS surface; as-deposited PLD-grown $Al_2O_3$ coating on 316L SS: (b) cross-section, (c) surface; (d) surface of PLD-grown $Al_2O_3$ coating after ion-irradiation (50 dpa).

### 3.2. Grazing Incidence X-Ray diffraction (GIXRD)

Fig. 3. presents GI XRD results of alumina coating recorded on the specimens in virgin state and after ion-irradiation to maximum dose (50 dpa). One can notice that in the diffraction patterns only peaks of austenitic steel are present. This indicates that both the as-deposited and ion-irradiated coatings are mainly amorphous (i.e. the volume fraction of crystalline nanodomains – assuming their existence - is too low to be recognized by GIXRD). The spectrum gathered from the virgin sample is consistent with the work of Garcia Ferré et *al.* [10].

Obtained results clearly suggest that phase composition of the coating subjected to even high ion-irradiation like 50 dpa at RT remains stable. Therefore, one can conclude that the alumina coating deposited by PLD technique remains amorphous even in the wide range of damage, at least for the room temperature tests.

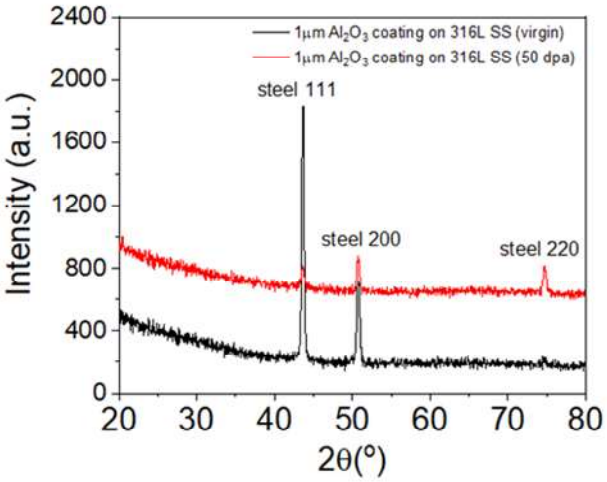


Fig. 3. GIXRD patterns of virgin and ion-irradiated alumina-coated sample.

### 3.3. Nanoindentation

#### 3.3.1. 316L

Fig. 4. compares the indentation depth dependence of nanohardness of 316L SS before and after irradiation (up to 50 dpa). Each point represents an average value of at least 10 indents performed at a certain force (starting from the left side of the Fig. 4., single points correspond respectively to forces of 0,2; 0,3; 0,4; 0,5; 0,7; 1; 1,5; 2; 3 and 4 mN). It is clear, that the hardness of the ion-modified sample is much higher than that of the pristine material across the whole range of forces.

One can see that the depth profile of the virgin sample shows well-known indentation size effect (ISE), wherein the hardness increases with decreasing indentation depth. This phenomenon can be observed in the whole indentation depths. The most widely used explanation of ISE is included in Nix-Gao model [36], which assumes that ISE is caused by the creation of geometrically necessary dislocations. It is particularly pronounced for sub-micrometer indentation depths, typically used to investigate ion-irradiated layers. Additionally, slightly lower values of hardness recorded at forces in the range 0,2 to 0,4 mN compared to the hardness recorded under force 0,5 mN can be observed. This is most likely

associated with surface conditions like roughness. The indentation depth profile of irradiated sample, intrinsically include three effects:

- Similarly to the hardness profile of non-irradiated material, there is an indentation size effect (ISE), but it overlaps with two following effects.
- Damage gradient effect (DGE) – due to non-uniform distribution of damage induced by irradiation (see Fig. 1.); the hardness initially increases with increasing level of damage, and after reaching a maximum level of damage decreases.
- Softer substrate effect (SSE) – after exceeding a certain indentation depth threshold, at which the plastic zone under the indenter tip begins to extend into the unirradiated volume of the material, measured values of the hardness starts to drops down.

Therefore, in the presented work overlapping of these effects should be taken into account. In order to determine the quantitative changes caused only by irradiation hardening, CSM (Continuous Stiffness Measurement) technique followed by application of suitable model [12,13,37–39] should be used. However, since presented research is preliminary and has comparative character and, finally, all measurements are affected by similar effects, this was not a concern of this study.

The comparison of curves allowed the selection of the optimum force to investigate the relationship between the irradiation dose and nanohardness of studied steel. One can see that the measurements performed at 0,3 mN load represent response of the damaged material. The measurements correspond to approximately 40 nm and 26 nm of plastic indentation depth for virgin and 50 dpa sample, respectively. One should note that all indentation depths performed at 0,3 mN, regardless of the material state are within approx. 20% thickness of the irradiated layer. Thus, we assumed that the presented results represent mainly the response of irradiated layer (no or minor influence of the unmodified bulk material is expected).

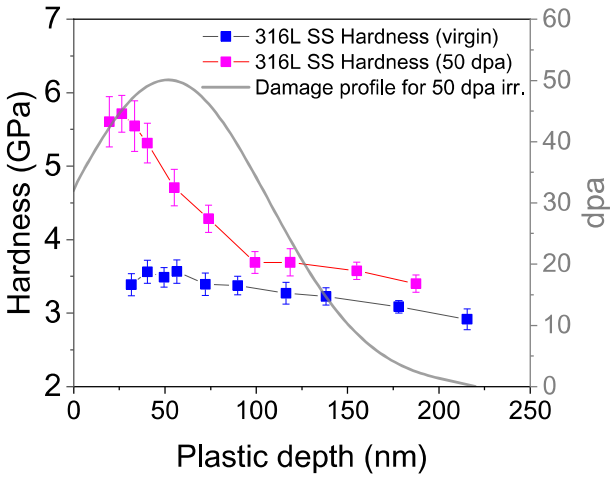


Fig. 4. Nanohardness of virgin and irradiated up to 50 dpa 316L SS plotted versus the plastic indentation depth. The gray line is the dose profile calculated by SRIM.

Fig. 5a. presents the nanohardness and elastic modulus of 316L SS as a function of irradiation dose expressed in dpa. The representative L-D curves of nanoindentation measurements are shown in Fig. 5b. As can be seen in Fig. 5a., the hardness of 316L steel increases with increasing level of damage, while the relationship for elastic modulus is opposite. The average hardness of the unirradiated sample is 3,55 ± 0,17 GPa, while for the sample irradiated up to 50 dpa, the hardness increases up to 5,71 ± 0,25 GPa. Obtained results are consistent with the investigation of T. Miura et *al.* [15] who reported hardness values of the virgin 316L SS to be (depending on grain orientation) around 3,0-3,5 GPa for unirradiated and 4,7-5,2 GPa for the irradiated up 10 dpa material. In this study, the hardness after 10 dpa irradiation is 4,72 ± 0,16 GPa. Observed changes in mechanical properties are the reflection of the changes introduced by the ions into microstructure. According to the literature [14,40], irradiation-induced hardening in fcc (face centered cubic) metals is attributed to the formation of various defects (including defect clusters, dislocation loops, dislocation lines, voids, bubbles and precipitates) which act as obstacles to the free movement of dislocations. The type, size, and density of the created defects depend, among other things, on irradiation temperature and dose [41–43]. Previously reported results on structural investigations of 300 series austenitic steels exposed

to irradiation, revealed that typical microstructure features formed due to irradiation at temperatures below 350 ºC are nano-scale black dots (small defect clusters, considered by many as small dislocation loops) [40,42–45], network dislocations [40,42] and dislocation loops [40,42–45].

It is well known that irradiation hardening of austenitic steel saturates at a few dpa [46–48]. This is linked to the microstructural evolution. Many authors [40,43,45] reported that both the loop number density and mean loop diameter increase up to a certain level of dpa (depending on irradiation conditions) and eventually saturate for higher doses. Mechanical results obtained in this study fit into this tendency. The hardness increase is rapid for doses under 3 dpa, and tends to saturate once this limit is achieved. The gradual hardness increase recorded for material irradiated in the range of 5 to 50 dpa has been attributed to minor microstructure alterations and to introduction of small quantities of carbon to the material during imperfect ion irradiation process. At the same time, the relatively high error in the recorder data (especially for Young modulus) most likely is related to the grain orientations and surface roughness. Finally, one cannot exclude stress introduced into the sample during polishing process. Despite these controversies, recorded results are in agreement with the literature and should be regarded as a first step in understating of the behavior of 316L/$Al_2O_3$ system upon irradiation.

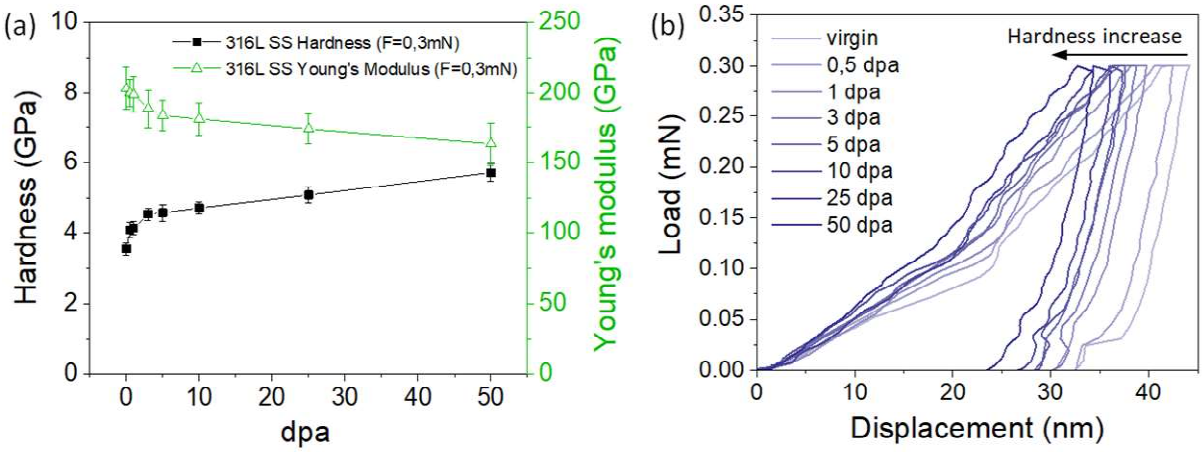

Fig. 5. (a) Nanohardness and Young's modulus versus irradiation dose for 316L SS. (b) Load versus displacement curves recorded before and after ion irradiation. Measurements performed at 0,3 mN.

### 3.3.2. $Al_2O_3$

The average nanoindentation hardness of alumina-coated samples before and after ion irradiation (to 50 dpa) is plotted as a function of the plastic depth, as shown in Fig. 6. Each plot data represents an average value of at least 10 indents performed at a certain force (starting from the left, single points correspond respectively to loads of 0,2; 0,4; 0,5; 1; 1,5; 2; 3; 5; 10 and 20 mN). When analyzing the curve representing the unirradiated sample (the blue curve), one can note that all measurements recorded below ~120 nm (i.e. forces lower than 5 mN) are affected by the surface artefacts, which is reflected in underestimated values of H. At the same time, application of higher forces (10-20 mN), led to plastic depths deep enough to start recording the response of the softer steel substrate. Therefore, if one wants to examine the mechanical properties of the 1 μm unirradiated coating itself, the use of 5 mN force would be recommended. The average values of hardness and Young's modulus of virgin $Al_2O_3$ coating determined in our tests at 5 mN are 9,9 ± 0,2 and 198,5 ± 4,1 GPa, respectively. The obtained results are in excellent agreement with the data of F. García Ferré et *al.* [5], who reported values of hardness and Young's modulus equal to 10 ± 1 GPa and 195 ± 9 GPa, respectively. At this point, the compatibility between mechanical properties of 316L SS and alumina coating is particularly notable. However, the aim of this study is to investigate the nanomechanical properties of the ion-irradiated coating. According to SRIM calculations (Fig. 1.), the radiation damage range for $Au^+$ 250 keV irradiation is about 60 nm. Therefore, if one wants to meet the requirement of keeping the indentation depths within 10-20% of the thickness of the measured layer, indentation to a maximum depth of 6-12 nm is necessary. However, the surface roughness of the studied coating was approx. 15-20 nm, so that 12 nm deep indents (0,2 mN load) are associated with significant errors and an underestimate

measured H, see Fig. 6. (first from the left two points). Therefore, the second lowest applied force of 0,4 mN was selected for analysis. However, one should bear in mind two consequences of this choice. Firstly, the recorded values of hardness (H) and Young's modulus (E) are still slightly undervalued (for the virgin sample H = 8,7 ± 0,2 GPa and E = 186 ± 9,7 GPa). Secondly, the measurements at 0,4 mN result in plastic depths of about 26 nm, so some influence of unirradiated volume of the material may be expected. Interestingly, in the region 100-150 nm depth, H of the irradiated specimen matches H of the virgin sample and in the region 50-100 nm is slightly lower. Taking into account irradiation depth of the alumina coated specimen, and impact of the unmodified substrate, one can postulate that at higher depths we record response of the unmodified bulk material. While recorded at lower depths data suggest softening. However, since the presented investigations are comparative and only a qualitative analysis was carried out, this hypothesis will be verified by investigating samples irradiated with higher energy.

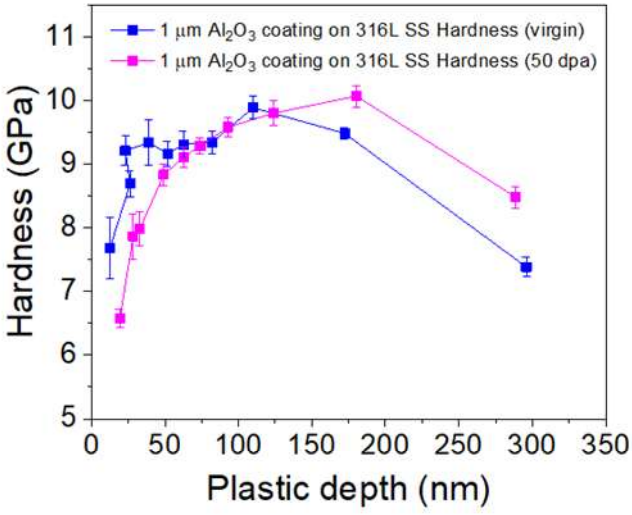


Fig. 6. Nanohardness of virgin and irradiated up to 50 dpa 1 μm $Al_2O_3$ coating on 316L SS plotted versus the plastic indentation depth.

The results of hardness and Young's modulus of alumina-coated samples as a function of irradiation dose are shown in Fig. 7a. The representative L-D curves of nanoindentation

measurements are presented in Fig. 7b. It is found that the hardness of all irradiated samples drops, but to a different extent depending on the dose. The initial rather significant decrease of hardness under irradiation at lower doses (up to 3 dpa) is followed by a slight and gradual increase under irradiation to higher doses. Concerning the Young's modulus values, the dependence is quite opposite; an initial rise under lower doses (up to 1 dpa) is followed by a significant drop under higher doses. Interestingly, the observed trends and scale of changes are completely different than those observed for 316L SS. Since amorphous materials do not possess long range order, irradiation does not generate vacancies and interstitials the way it does with crystalline materials. According to previous studies [49–53], changes in mechanical behavior of amorphous materials due to irradiation are predominantly caused by: (i) fluctuations in free volume (which is a loosely packed region on the atomic scale), (ii) radiation-induced crystallization and (iii) changes in bonding topology.

F. García Ferré et *al.* proved [4,9,10] that in PLD-grown $Al_2O_3$ coatings, irradiation initially induces an amorphous-to-crystalline transformation, while extended irradiation induces a grain growth which increases with increasing dpa. As for the nanomechanical properties, it was found that the initial transformation is accompanied by a significant hardness increase (from $H_{virgin}$ = 9,9 ± 0,2 GPa to $H_{20dpa}$ = 17,8 ± 0,2 GPa), while subsequent grain growth results in a softening of the material ($H_{40dpa}$ = 17,2 ± 1,2 GPa, $H_{150dpa}$ = 15,9 ± 1,6 GPa), in accordance to the Hall-Petch relationship. The (reduced) Young's modulus was shown to increase monotonically with increasing dose (from $E_{r,20dpa}$ = 205 ± 0,7 GPa to $E_{r,150dpa}$ = 245 ± 10 GPa). However, since no evidence of significant hardening was observed in this study, we assume that crystallization did not occur. This finding is fully consistent with GIXRD analysis (see Fig. 3.). According to [9,10], the onset of crystallization depends on the dose, dose rate and temperature. The temperature component plays a crucial role, because it can trigger phase transformation entirely independently. α-$Al_2O_3$ is the only thermodynamically stable phase of alumina [54–56]. Any other forms i.e. amorphous or

crystalline polymorphs (γ, δ, η, χ, θ and κ) are metastable. Therefore, once the certain thermal activation energy is achieved, metastable material commence phase transformation. In the study performed by N. Yu et *al.* [57] it has been demonstrated that the recrystallization rate of thin alumina films (which is induced by ion beam) is the temperature dependent factor. The higher the temperature (in the range of 400 to 600 °C) the faster the regrowth process under irradiation. One must remember that in the investigations of F. García Ferré et *al.*, irradiations were carried out at 600 ºC, while RT ion implantations were performed in this study. Therefore, we believe that the disparities observed between our and reported studies arise from different irradiation conditions. In order to answer this question, TEM studies on samples irradiated at room temperature with high energy Au-ions have been started.

A similar mechanical response to irradiation was observed in ion irradiated metallic glass $Ni_{50}Nb_{10}Zr_{15}Ti_{15}Pt_{7.5}Cu_{2.5}$ obtained by Y.H. Qiu et *al.* [58], where Positron annihilation Doppler broadening results showed that low dose irradiation destroys the short range order and introduce extensive free volume, while high dose irradiation promote the formation of local order structure consuming the free volume (in order to confirm this hypothesis, TEM studies are ongoing). The comparison of positron annihilation DB with nanoindentation measurements reveals a close relationship between changes in free volume and mechanical properties in metallic glasses. One can conclude that increase in free volume results in a decrease in hardness. These fluctuations in the free volume content are one of the possible explanations for the alteration of mechanical properties observed in this study. On the other hand, it should be pointed out that TEM studies of the investigated $Al_2O_3$ [4,5,9,10] showed that as-deposited coatings are composed of a dual phase structure, and that although the overall structure is predominantly amorphous, some very low fraction of γ-$Al_2O_3$ can be present. This may lead to other mechanisms of plastic deformation and alternative behavior under irradiation. Results reported in the work of Wei et *al.* [50] concerning the evolution of microstructure and mechanical properties in bulk metallic glass composite (BMGC)

($Cu_{48}Zr_{48}Al_4$ consisting of a glassy matrix and crystalline phases) due to irradiation suggest that in BMGCs, simultaneous softening (caused by increase of the free volume) and hardening effects (linked to phase transformation) in amorphous and crystalline regions, respectively, may occur. However in that study the increase of hardness in amorphous regions was accompanied by the rise of Young's modulus, while in our results the direction of hardness and elastic modulus changes were opposite. There is also a possibility that observed changes in hardness are simply due to the sputtering of light alumina elements by gold ions during irradiation process, resulting in the decrease of density of near-surface region. This would mean that irradiation up to 50 dpa at RT in no way affects the mechanical properties of alumina grown by PLD.

As the investigated alumina possesses a complex and unusual structure, and because of the lack of comprehensive understanding (especially from the structural point of view) of the response of amorphous materials to irradiation, proposed explanations of the observed trends should not be considered as the only reasonable ones. Additional data are needed to understand this subject matter. Reported results should be taken as a starting point and background for further complex structural and mechanical investigations such as combinations of higher energy irradiation, new nanoindentation campaign (both in room and at high temperature), Raman analysis, GI XRD and finally HR TEM measurements. Actually, such research is currently ongoing. GI XRD, Raman spectroscopy and HR TEM are complementary to each other and serve us to develop deeper understanding of irradiation triggered microstructural changes and to design optimized methodology for further studies. In case of low energy (and therefore usually shallow) ion irradiated non-metallic samples, Raman analysis appears to be a promising method, because spectra can be collected from a very small volume of the material. Transmission Electron Microscopy (TEM) seems to be suitable for initial verification of the validity of the postulated phenomena. If assumptions concerning the microstructural ordering/disordering are correct, we expect that TEM images

of ion-irradiated samples will not reveal any obvious changes compared to images of virgin material. This was the case in the study performed by A. G. Perez-Bergquist et *al.* [59] concerning the effects of ion irradiation of $Zr_{52.5}Cu_{17.9}Ni_{14.6}Al_{10}Ti_5$ (BAM-11) metallic glass. In the future, authors will consider implementation of the Positron Annihilation Spectroscopy technique which in terms of detecting changes in free volume concentrations in amorphous materials, gives satisfactory results [58,60–62].

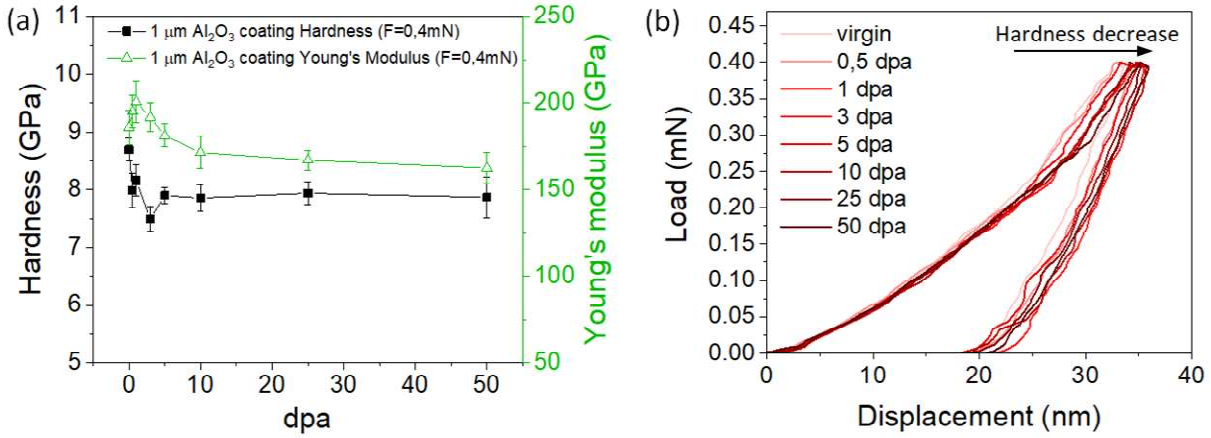


Fig. 7. (a) Nanohardness and Young's modulus versus irradiation dose for 1 μm $Al_2O_3$ coating on 316L SS. (b) Load versus displacement curves recorded before and after ion irradiation. Measurements performed at 0,4 mN.

Since the investigated coating is meant for fuel cladding applications, its tribological behaviour needs to be assessed as well. In this study, two parameters commonly regarded as reliable indicators of wear resistance are considered. These are: the ratio of hardness and elastic modulus (H/E) [5,63–65] and the ratio of plastic to total indentation work ($W_{pl}/W_{tot}$) [5,64,65] also called "microhardness dissipation parameter" (MDP). One must remember that the choice of H/E or MDP for wear resistance evaluation is more justified in stable and adhesive wear conditions, respectively [5].

Presented studies (Fig. 8.) shows that the MDP varies from 0.566 ± 0.024 for as-deposited condition, to 0.71 ± 0.017 for 3 dpa. These results indicate that the robustness of the PLD-grown alumina against adhesive wear is good and can be noticeably improved by irradiation.

Regarding the H/E ratio, one can see that the parameter decreases under lower dose irradiation (from 0.047 ± 0.003 for as-deposited condition, to 0.039 ± 0.002 for 3 dpa), and restores to the level of unirradiated sample under higher dose irradiation. Reported data indicate good coating performance in stable wear conditions, even despite slight degradation under modest irradiation doses.

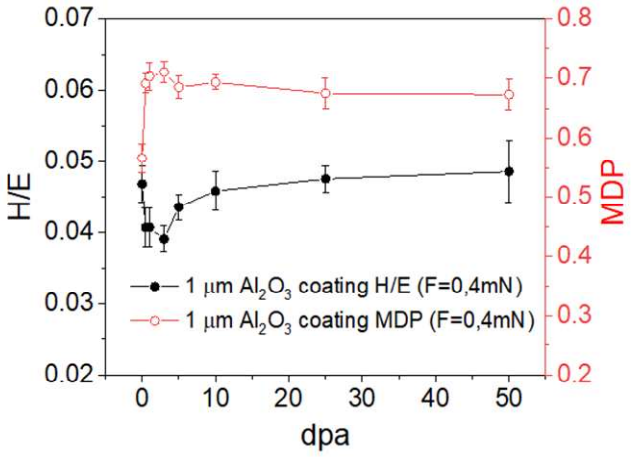


Fig. 8. H/E and MDP parameters versus irradiation dose for 1 μm $Al_2O_3$ coating on 316L SS.

## 4. Conclusions

In the present study, examinations of nanomechanical properties of both the PLD-grown $Al_2O_3$ coating on 316L SS and the 316L SS substrate itself, in virgin and irradiated states, have been performed. Irradiations were carried out (250 keV $Au^+$ and 150 keV $Fe^{2+}$ for alumina coating and steel, respectively) at room temperature leading to damage doses ranging from 0,5 to 50 dpa. Nanoindentation investigations revealed that the hardness of the studied nanocrystalline $Al_2O_3$/a-$Al_2O_3$ composite coating drops slightly due to irradiation. However, the scale of the decrease depends from the dose. The only minor changes recorded even for high dpa levels suggest that PLD-grown $Al_2O_3$ coating can maintain stable mechanical properties over a wide range of doses, which makes it attractive in terms of nuclear applications (especially in the IV Generation systems). At the same time, the well-known radiation hardening effect of 316L SS was observed. These results suggest that radiation

response mechanisms of amorphous materials are quite different from those found and relatively well known for crystalline materials, for examples as proved by GI XRD data, irradiation even to high doses does not affect the structure of the coating.

**Acknowledgment**

The research leading to these results was carried out in the frame of EERA Joint Programme on Nuclear Materials and is partly funded by the European Commission HORIZON 2020 Framework Programme under grant agreement No. 755269.

**References:**


[1] P. Lorusso, S. Bassini, A. Del Nevo, I. Di Piazza, F. Giannetti, M. Tarantino, M. Utili, GEN-IV LFR development: Status & perspectives, Prog. Nucl. Energy. 105 (2018) 318–331. doi:10.1016/j.pnucene.2018.02.005.

[2] A. Weisenburger, A. Gessi, A. Jianu, M. Del Giacco, R. Fetzer, A. Heinzel, G. Müller, P. Agostini, Materials for ALFRED and ELFR selection and challenges, in: n.d. https://inis.iaea.org/search/search.aspx?orig_q=RN:45089566 (accessed July 4, 2019).

[3] G. Grasso, C. Petrovich, D. Mattioli, C. Artioli, P. Sciora, D. Gugiu, G. Bandini, E. Bubelis, K. Mikityuk, The core design of ALFRED, a demonstrator for the European lead-cooled reactors, Nucl. Eng. Des. 278 (2014) 287–301. doi:10.1016/j.nucengdes.2014.07.032.

[4] F.G. Ferré, A. Mairov, D. Iadicicco, M. Vanazzi, S. Bassini, M. Utili, M. Tarantino, M. Bragaglia, F.R. Lamastra, F. Nanni, L. Ceseracciu, Y. Serruys, P. Trocellier, L. Beck, K. Sridharan, M.G. Beghi, F. Di Fonzo, Corrosion and radiation resistant nanoceramic coatings for lead fast reactors, Corros. Sci. 124 (2017) 80–92. doi:10.1016/j.corsci.2017.05.011.

[5] F. García Ferré, E. Bertarelli, A. Chiodoni, D. Carnelli, D. Gastaldi, P. Vena, M.G. Beghi, F. Di Fonzo, The mechanical properties of a nanocrystalline Al2O3/a-Al2O3composite coating measured by nanoindentation and Brillouin spectroscopy, Acta Mater. 61 (2013) 2662–2670. doi:10.1016/j.actamat.2013.01.050.

[6] D. Iadicicco, M. Vanazzi, F.G. Ferré, B. Paladino, S. Bassini, M. Utili, F. Di Fonzo, Multifunctional nanoceramic coatings for future generation nuclear systems, Fusion Eng. Des. (2019) 0–1. doi:10.1016/j.fusengdes.2019.03.004.

[7] D. Iadicicco, S. Bassini, M. Vanazzi, P. Mu, A. Moro, Efficient hydrogen and deuterium permeation reduction in Al 2 O 3 coatings with enhanced radiation tolerance and corrosion resistance, (2018). doi:10.1088/1741-4326/aadd1d.

[8] F. García Ferré, M. Ormellese, F. Di Fonzo, M.G. Beghi, Advanced Al2O3 coatings for high temperature operation of steels in heavy liquid metals: A preliminary study, Corros. Sci. 77 (2013) 375–378. doi:10.1016/j.corsci.2013.07.039.

[9] F. Garciá Ferré, A. Mairov, L. Ceseracciu, Y. Serruys, P. Trocellier, C. Baumier, O. Kaïtasov, R. Brescia, D. Gastaldi, P. Vena, M.G. Beghi, L. Beck, K. Sridharan, F. Di Fonzo, Radiation endurance in Al2O3nanoceramics, Sci. Rep. 6 (2016) 1–9. doi:10.1038/srep33478.

[10] F. García Ferré, A. Mairov, M. Vanazzi, Y. Serruys, F. Leprêtre, L. Beck, L. Van Brutzel, A. Chartier, M.G. Beghi, K. Sridharan, F. Di Fonzo, Extreme ion irradiation of oxide nanoceramics: Influence of the irradiation spectrum, Acta Mater. 143 (2018) 156–165. doi:10.1016/j.actamat.2017.10.011.

[11] G.S. Was, Z. Jiao, E. Getto, K. Sun, A.M. Monterrosa, S.A. Maloy, O. Anderoglu, B.H. Sencer, M. Hackett, Emulation of reactor irradiation damage using ion beams, Scr. Mater. 88 (2014) 33–36. doi:10.1016/j.scriptamat.2014.06.003.

[12] A. Kareer, A. Prasitthipayong, D. Krumwiede, D.M. Collins, P. Hosemann, S.G. Roberts, An analytical method to extract irradiation hardening from nanoindentation hardness-depth curves, J. Nucl. Mater. 498 (2018) 274–281. doi:10.1016/j.jnucmat.2017.10.049.

[13] X. Xiao, Q. Chen, H. Yang, H. Duan, J. Qu, A mechanistic model for depth-dependent hardness of ion irradiated metals, J. Nucl. Mater. 485 (2017) 80–89. doi:10.1016/j.jnucmat.2016.12.039.

[14] G.S. Was, Fundamentals od Radiation Material Science, 2007. doi:10.15713/ins.mmj.3.

[15] T. Miura, K. Fujii, K. Fukuya, K. Takashima, Influence of crystal orientation on hardness and nanoindentation deformation in ion-irradiated stainless steels, J. Nucl. Mater. 417 (2011) 984–987. doi:10.1016/j.jnucmat.2010.12.197.

[16] C. Heintze, C. Recknagel, F. Bergner, M. Hernández-Mayoral, A. Kolitsch, Ion-irradiation-induced damage of steels characterized by means of nanoindentation, Nucl. Instruments Methods Phys. Res. Sect. B Beam Interact. with Mater. Atoms. 267 (2009) 1505–1508. doi:10.1016/j.nimb.2009.01.122.

[17] H.F. Huang, J.J. Li, D.H. Li, R.D. Liu, G.H. Lei, Q. Huang, L. Yan, TEM, XRD and nanoindentation characterization of Xenon ion irradiation damage in austenitic stainless steels, J. Nucl. Mater. 454 (2014) 168–172. doi:10.1016/j.jnucmat.2014.07.033.

[18] J. Jagielski, L. Thomé, P. Aubert, O. Maciejak, A. Piatkowska, M. Romaniec, S. Moll, Nanomechanical measurements of irradiated layers: Methodology, possibilities and pitfalls, Vacuum. 83 (2009) 12–15. doi:10.1016/j.vacuum.2009.01.013.

[19] L. Meng, B. Raghavan, O. Bartier, X. Heentarnot, G. Mauvoisin, P. Breitkopf, An objective meta-modeling approach for indtion-based material characterization, Mech. Mater. (2017). doi:10.1016/j.mechmat.2017.01.011.

[20] L. Meng, P. Breitkopf, B. Raghavan, G. Mauvoisin, O. Bartier, X. Hernot, On the study of mystical materials identified by indentation on power law and Voce hardening solids, Int. J. Mater. Form. 12 (2019) 587–602. doi:10.1007/s12289-018-1436-1.

[21] M. Frelek-Kozak, L. Kurpaska, M. Lesniak, I. Jozwik, J. Jagielski, Mechanical and structural properties of ODS RAF steels submitted to low-energy ions irradiation, Fusion Eng. Des. 127 (2018) 54–59. doi:10.1016/j.fusengdes.2017.12.006.

[22] L. Kurpaska, M. Gapinska, J. Jasinski, M. Lesniak, M. Sitarz, K. Nowakowska-Langier, J. Jagielski, K. Wozniak, Influence of Ar-irradiation on structural and nanomechanical properties of pure zirconium measured by means of GIXRD and nanoindentation techniques, J. Mol. Struct. 1126 (2016) 226–231. doi:10.1016/j.molstruc.2016.03.053.

[23] L. Kurpaska, Nanomechanical investigation of ion implanted single crystals – Challenges, possibilities and pitfall traps related to nanoindentation, Nucl. Instruments Methods Phys. Res. Sect. B Beam Interact. with Mater. Atoms. 409 (2017) 171–174. doi:10.1016/j.nimb.2017.04.052.

[24] A. Lupinacci, K. Chen, Y. Li, M. Kunz, Z. Jiao, G.S. Was, M.D. Abad, A.M. Minor, P. Hosemann, Characterization of ion beam irradiated 304 stainless steel utilizing nanoindentation and Laue microdiffraction, J. Nucl. Mater. 458 (2015) 70–76.

doi:10.1016/j.jnucmat.2014.11.050.

[25] S.J. Zinkle, Effect of irradiation spectrum on the microstructural evolution in ceramic insulators, J. Nucl. Mater. 219 (1995) 113–127. doi:10.1016/0022-3115(94)00662-8.

[26] T. Aruga, Y. Katano, T. Ohmichi, S. Okayasu, Y. Kazumata, Amorphization behaviors in polycrystalline alumina irradiated with energetic iodine ions, Nucl. Instruments Methods Phys. Res. Sect. B Beam Interact. with Mater. Atoms. (2000). doi:10.1016/S0168-583X(99)00800-9.

[27] V.A. Skuratov, S.J. Zinkle, A.E. Efimov, K. Havancsak, Swift heavy ion-induced modification of Al 2 O 3 and MgO surfaces, in: Nucl. Instruments Methods Phys. Res. Sect. B Beam Interact. with Mater. Atoms, 2003. doi:10.1016/S0168-583X(02)02197-3.

[28] N. Khalfaoui, J.P. Stoquert, F. Haas, C. Traumann, A. Meftah, M. Toulemonde, Damage creation threshold of Al 2O 3 under swift heavy ion irradiation, in: Nucl. Instruments Methods Phys. Res. Sect. B Beam Interact. with Mater. Atoms, 2012. doi:10.1016/j.nimb.2011.11.047.

[29] P. Angerer, S. Strobl, Equi-penetration grazing incidence X-ray diffraction method: Stress depth profiling of ground silicon nitride, Acta Mater. (2014). doi:10.1016/j.actamat.2014.06.015.

[30] W.C. Oliver, G.M. Pharr, An improved technique for determining hardness and elastic modulus using load and displacement sensing indentation experiments, J. Mater. Res. 7 (1992) 1564–1583. doi:10.1557/JMR.1992.1564.

[31] M.M. Morshed, B.P. McNamara, D.C. Cameron, M.S.J. Hashmi, Effect of surface treatment on the adhesion of DLC film on 316L stainless steel, Surf. Coatings Technol. 163–164 (2003) 541–545. doi:10.1016/S0257-8972(02)00619-9.

[32] P. Hosemann, D. Kiener, Y. Wang, S.A. Maloy, Issues to consider using nano indentation on shallow ion beam irradiated materials, J. Nucl. Mater. 425 (2012) 136–139. doi:10.1016/j.jnucmat.2011.11.070.

[33] A.H. Mir, I. Monnet, M. Toulemonde, S. Bouffard, C. Jegou, S. Peuget, Mono and sequential ion irradiation induced damage formation and damage recovery in oxide glasses: Stopping power dependence of the mechanical properties, J. Nucl. Mater. (2016). doi:10.1016/j.jnucmat.2015.12.004.

[34] S. Peuget, P.Y. Noël, J.L. Loubet, S. Pavan, P. Nivet, A. Chenet, Effects of deposited nuclear and electronic energy on the hardness of R7T7-type containment glass, Nucl. Instruments Methods Phys. Res. Sect. B Beam Interact. with Mater. Atoms. (2006). doi:10.1016/j.nimb.2005.12.053.

[35] A.C. Fischer-Cripps, Critical review of analysis and interpretation of nanoindentation test data, Surf. Coatings Technol. 200 (2006) 4153–4165. doi:10.1016/j.surfcoat.2005.03.018.

[36] W.D. Nix, H.J. Gao, Indentation size effects in crystalline materials: A law for strain gradient plasticity, J. Mech. Phys. Solids. 46 (1998) 411–425. doi:10.1016/s0022-5096(97)00086-0.

[37] K. Yabuuchi, Y. Kuribayashi, S. Nogami, R. Kasada, A. Hasegawa, Evaluation of

irradiation hardening of proton irradiated stainless steels by nanoindentation, J. Nucl. Mater. 446 (2014) 142–147. doi:10.1016/j.jnucmat.2013.12.009.

[38] C. Heintze, F. Bergner, S. Akhmadaliev, E. Altstadt, Ion irradiation combined with nanoindentation as a screening test procedure for irradiation hardening, J. Nucl. Mater. 472 (2016) 196–205. doi:10.1016/j.jnucmat.2015.07.023.

[39] P.P. Liu, F.R. Wan, Q. Zhan, A model to evaluate the nano-indentation hardness of ion-irradiated materials, Nucl. Instruments Methods Phys. Res. Sect. B Beam Interact. with Mater. Atoms. 342 (2015) 13–18. doi:10.1016/j.nimb.2014.09.012.

[40] G.S. Was, P.L. Andresen, Radiation damage to structural alloys in nuclear power plants: Mechanisms and remediation, 2014. doi:10.1533/9780857097552.2.355.

[41] R.J.M. Konings, Comprehensive Nuclear Materials, Volume 4_ Radiation Effects in Structural and Functional Materials for Fission and Fusion Reactors 4, 2012. doi:10.1016/B978-0-12-381373-2.11001-4.

[42] S.J. Zinkle, P.J. Maziasz, R.E. Stoller, Dose dependence of the microstructural evolution, J. Nucl. Mater. 206 (2008) 266–286.

[43] A. Etienne, M. Hernández-Mayoral, C. Genevois, B. Radiguet, P. Pareige, Dislocation loop evolution under ion irradiation in austenitic stainless steels, J. Nucl. Mater. 400 (2010) 56–63. doi:10.1016/j.jnucmat.2010.02.009.

[44] N. Hashimoto, E. Wakai, J.P. Robertson, Damage structure in austenitic stainless steel 316LN irradiated at low temperature in the HFIR, J. Electron Microsc. (Tokyo). 48 (1999) 575–580. doi:10.1093/oxfordjournals.jmicro.a023718.

[45] C. Pokor, Y. Brechet, P. Dubuisson, J.P. Massoud, A. Barbu, Irradiation damage in 304 and 316 stainless steels: Experimental investigation and modeling. Part I: Evolution of the microstructure, J. Nucl. Mater. 326 (2004) 19–29. doi:10.1016/j.jnucmat.2003.11.007.

[46] K. Yabuuchi, Y. Kuribayashi, S. Nogami, R. Kasada, A. Hasegawa, Evaluation of irradiation hardening of proton irradiated stainless steels by nanoindentation, J. Nucl. Mater. 446 (2014) 142–147. doi:10.1016/j.jnucmat.2013.12.009.

[47] J.P. Robertson, I. Ioka, A.F. Rowcliffe, M.L. Grossbeck-, S. Jitsukawa, 316 Stainless Steel After Low Temperature Neutron, (1997).

[48] C. Pokor, Y. Brechet, P. Dubuisson, J.P. Massoud, X. Averty, Irradiation damage in 304 and 316 stainless steels: Experimental investigation and modeling. Part II: Irradiation induced hardening, J. Nucl. Mater. 326 (2004) 30–37. doi:10.1016/j.jnucmat.2003.12.008.

[49] Y.H. Qiu, C. Xu, E.G. Fu, P.P. Wang, J.L. Du, Z.Y. Hu, X.Q. Yan, X.Z. Cao, Y.G. Wang, L. Shao, Mechanisms for the free volume tuning the mechanical properties of metallic glass through ion irradiation, Intermetallics. 101 (2018) 173–178. doi:10.1016/j.intermet.2018.08.006.

[50] Y. Wei, K. Zhang, B. Wei, Z. Zhao, J. Yuan, Microstructural evolution and mechanical properties in Cu 48 Zr 48 Al 4 bulk metallic glass composites induced by He + ion irradiation, Nucl. Instruments Methods Phys. Res. Sect. B Beam Interact. with Mater. Atoms. 428 (2018) 17–23. doi:10.1016/j.nimb.2018.05.003.

[51] Q. Su, S. Inoue, M. Ishimaru, J. Gigax, T. Wang, H. Ding, M.J. Demkowicz, L. Shao, M. Nastasi, Helium Irradiation and Implantation Effects on the Structure of Amorphous Silicon Oxycarbide, Sci. Rep. 7 (2017) 1–8. doi:10.1038/s41598-017-04247-x.

[52] X.L. Bian, G. Wang, H.C. Chen, L. Yan, J.G. Wang, Q. Wang, P.F. Hu, J.L. Ren, K.C. Chan, N. Zheng, A. Teresiak, Y.L. Gao, Q.J. Zhai, J. Eckert, J. Beadsworth, K.A. Dahmen, P.K. Liaw, Manipulation of free volumes in a metallic glass through Xe-ion irradiation, Acta Mater. (2016). doi:10.1016/j.actamat.2016.01.002.

[53] M. Nastasi, Q. Su, L. Price, J.A. Colón Santana, T. Chen, R. Balerio, L. Shao, Superior radiation tolerant materials: Amorphous silicon oxycarbide, J. Nucl. Mater. 461 (2015) 200–205. doi:10.1016/j.jnucmat.2015.02.039.

[54] I. Levin, D. Brandon, Metastable Alumina Polymorphs: Crystal Structures and Transition Sequences, J. Am. Ceram. Soc. 81 (2010) 1995–2012. doi:10.1111/j.1151-2916.1998.tb02581.x.

[55] V. Edlmayr, M. Moser, C. Walter, C. Mitterer, Thermal stability of sputtered Al2O3 coatings, Surf. Coatings Technol. (2010). doi:10.1016/j.surfcoat.2009.10.002.

[56] P. Zeman, Š. Zuzjaková, J. Blažek, R. Čerstvý, J. Musil, Thermally activated transformations in metastable alumina coatings prepared by magnetron sputtering, Surf. Coatings Technol. 240 (2014) 7–13. doi:10.1016/j.surfcoat.2013.12.004.

[57] N. Yu, M. Nastasi, Ion beam induced epitaxial recrystallization of alumina thin films deposited on sapphire, Nucl. Inst. Methods Phys. Res. B. (1995). doi:10.1016/0168-583X(95)00773-3.

[58] Y.H. Qiu, C. Xu, E.G. Fu, P.P. Wang, J.L. Du, Z.Y. Hu, X.Q. Yan, X.Z. Cao, Y.G. Wang, L. Shao, Mechanisms for the free volume tuning the mechanical properties of metallic glass through ion irradiation, Intermetallics. (2018). doi:10.1016/j.intermet.2018.08.006.

[59] A.G. Perez-Bergquist, H. Bei, K.J. Leonard, Y. Zhang, S.J. Zinkle, Effects of ion irradiation on Zr52.5Cu17.9Ni 14.6Al10Ti5 (BAM-11) bulk metallic glass, Intermetallics. (2014). doi:10.1016/j.intermet.2014.04.016.

[60] L. Yang, H.Y. Li, P.W. Wang, S.Y. Wu, G.Q. Guo, B. Liao, Q.L. Guo, X.Q. Fan, P. Huang, H.B. Lou, F.M. Guo, Q.S. Zeng, T. Sun, Y. Ren, L.Y. Chen, Structural responses of metallic glasses under neutron irradiation, Sci. Rep. 7 (2017) 1–13. doi:10.1038/s41598-017-17099-2.

[61] L.Y. Chen, A.D. Setyawan, H. Kato, A. Inoue, G.Q. Zhang, J. Saida, X.D. Wang, Q.P. Cao, J.Z. Jiang, Free-volume-induced enhancement of plasticity in a monolithic bulk metallic glass at room temperature, Scr. Mater. (2008). doi:10.1016/j.scriptamat.2008.02.025.

[62] C.A. Schuh, T.C. Hufnagel, U. Ramamurty, Mechanical behavior of amorphous alloys, Acta Mater. 55 (2007) 4067–4109. doi:10.1016/j.actamat.2007.01.052.

[63] A. Leyland, A. Matthews, On the significance of the H/E ratio in wear control: A nanocomposite coating approach to optimised tribological behaviour, Wear. 246 (2000) 1–11. doi:10.1016/S0043-1648(00)00488-9.

[64] B.D. Beake, J.F. Smith, A. Gray, G.S. Fox-rabinovich, S.C. Veldhuis, J.L. Endrino, Investigating the correlation between nano-impact fracture resistance and hardness / modulus ratio from nanoindentation at 25 – 500 ° C and the fracture resistance and lifetime of cutting tools with Ti 1 − x Al x N ( x = 0 . 5 and 0 . 67 ) PVD coatings in, 201 (2007) 4585–4593. doi:10.1016/j.surfcoat.2006.09.118.

[65] G.S. Fox-rabinovich, B.D. Beake, J.L. Endrino, S.C. Veldhuis, R. Parkinson, Effect of mechanical properties measured at room and elevated temperatures on the wear resistance of cutting tools with TiAlN and AlCrN coatings, 200 (2006) 5738–5742. doi:10.1016/j.surfcoat.2005.08.132.

List of figure captions

Fig. 1. Simulated irradiation damage (in dpa) as a function of target depth for: (a) 150 keV $Fe^{2+}$ ions in 316L SS; (b) 250 keV $Au^{+}$ ions in $Al_2O_3$ coating (1 μm thickness).

Fig. 2. SEM images of: (a) etched 316L SS surface; as-deposited PLD-grown $Al_2O_3$ coating on 316L SS: (b) cross-section, (c) surface; (d) surface of PLD-grown $Al_2O_3$ coating after ion-irradiation (50 dpa).

Fig. 3. GIXRD patterns of virgin and ion-irradiated alumina-coated sample.

Fig. 4. Nanohardness of virgin and irradiated up to 50 dpa 316L SS plotted versus the plastic indentation depth. The gray line is the dose profile calculated by SRIM.

Fig. 5. (a) Nanohardness and Young's modulus versus irradiation dose for 316L SS. (b) Load versus displacement curves recorded before and after ion irradiation. Measurements performed at 0,3 mN.

Fig. 6. Nanohardness of virgin and irradiated up to 50 dpa 1 μm $Al_2O_3$ coating on 316L SS plotted versus the plastic indentation depth.

Fig. 7. (a) Nanohardness and Young's modulus versus irradiation dose for 1 μm $Al_2O_3$ coating on 316L SS. (b) Load versus displacement curves recorded before and after ion irradiation. Measurements performed at 0,4 mN.

Fig. 8. H/E and MDP parameters versus irradiation dose for 1 μm $Al_2O_3$ coating on 316L SS.

Figures

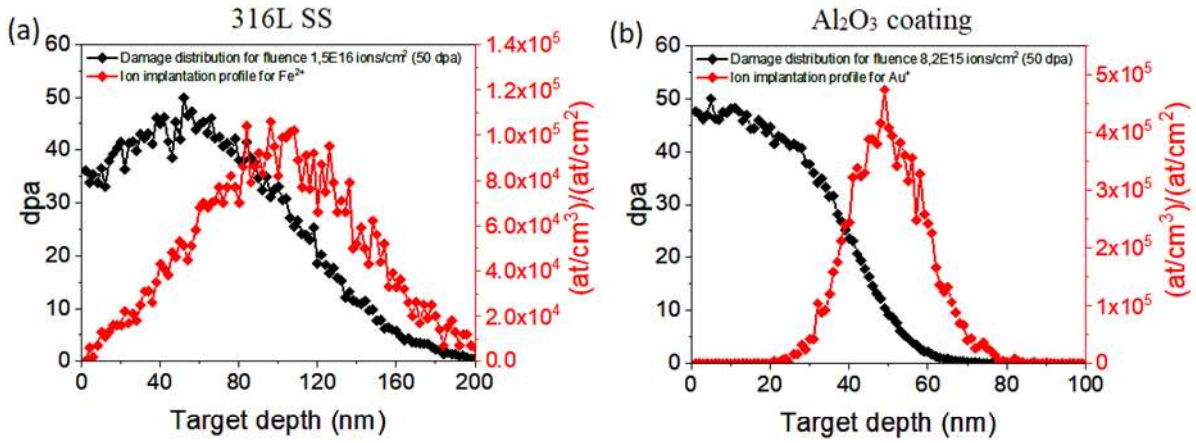


Fig. 1.

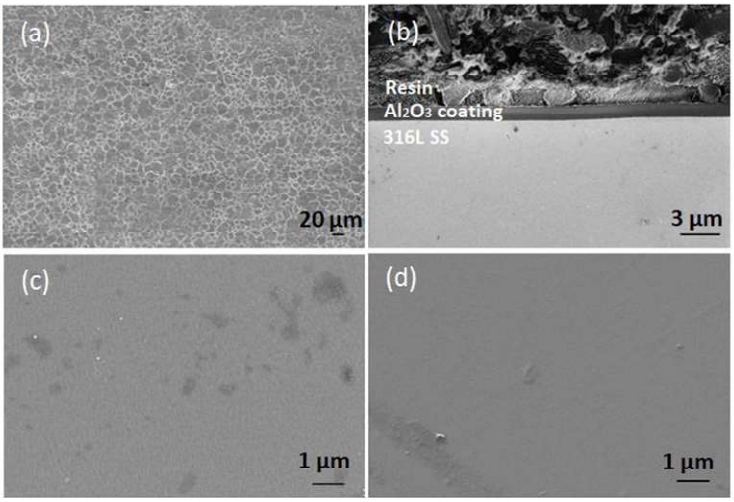


Fig. 2.

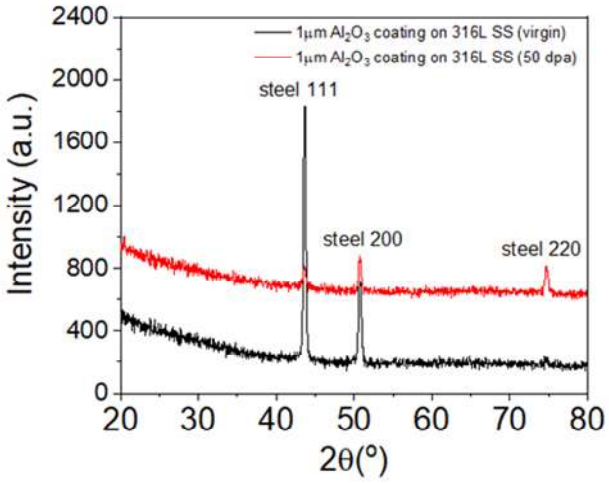


Fig. 3.

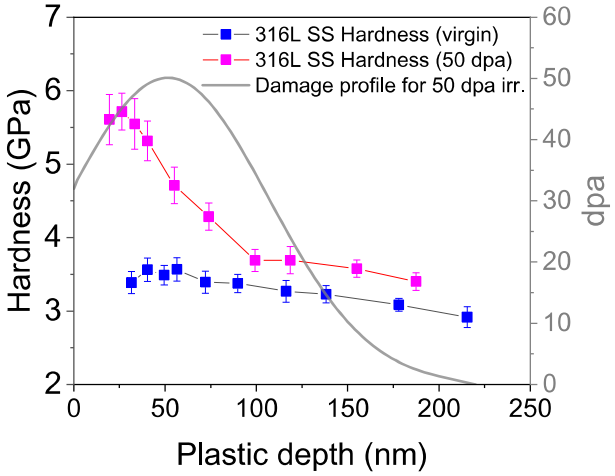


Fig. 4.

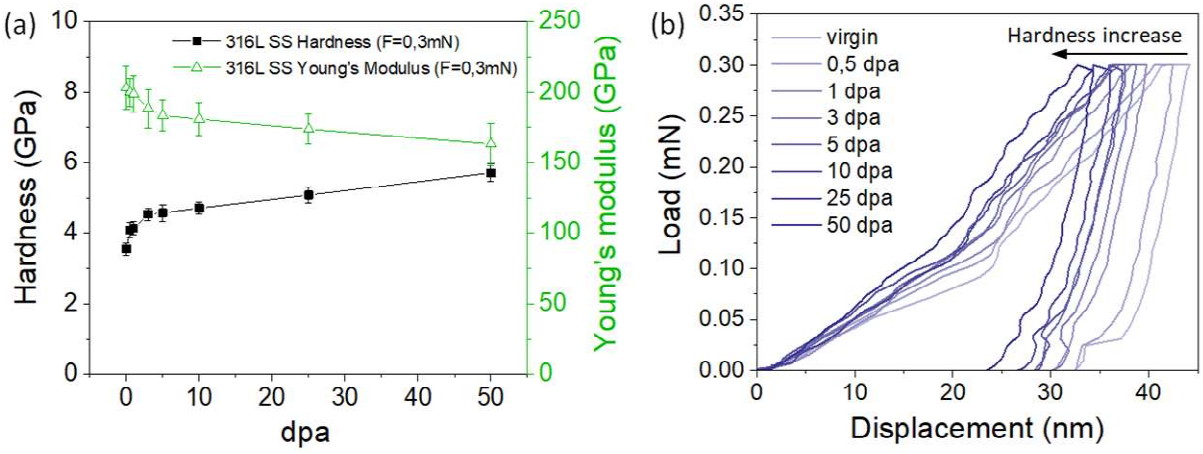


Fig. 5.

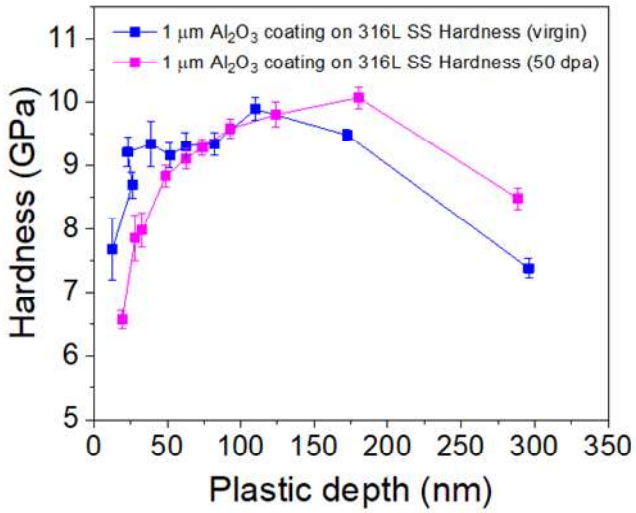
1 μm Al2O3 coating on 316L SS Hardness (virgin)
1 μm Al2O3 coating on 316L SS Hardness (50 dpa)
Hardness (GPa)
Plastic depth (nm)

Fig. 6.

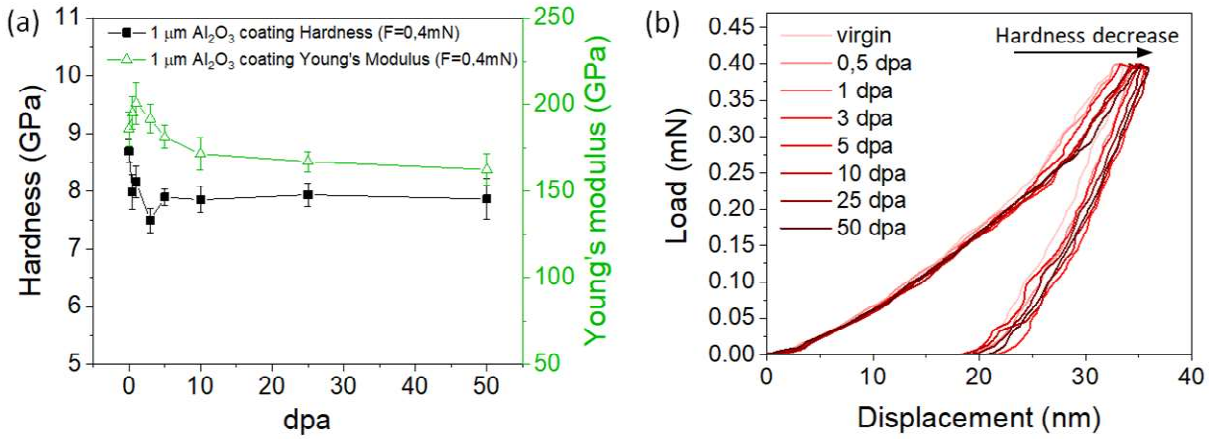
(a)
1 μm Al2O3 coating Hardness (F=0,4mN)
1 μm Al2O3 coating Young's Modulus (F=0.4mN)
Hardness (GPa)
Young's modulus (GPa)
dpa
(b)
virgin
0,5 dpa
1 dpa
3 dpa
5 dpa
10 dpa
25 dpa
50 dpa
Hardness decrease
Load (mN)
Displacement (nm)

Fig. 7.

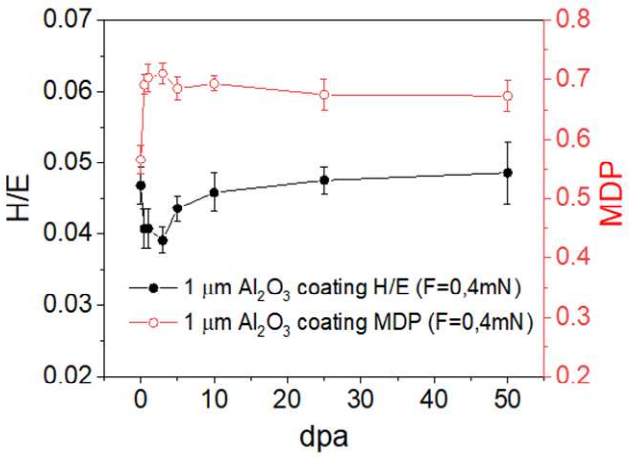
H/E
MDP
1 μm Al2O3 coating H/E (F=0,4mN)
1 μm Al2O3 coating MDP (F=0,4mN)
dpa

Fig. 8.